

Gravimetric evidences of active faults and underground structure of the Cheliff seismogenic basin (Algeria)

Abdesslam Abtout, Hassina Boukerbout, Boualem Bouyahiaoui, Dominique Gibert

► **To cite this version:**

Abdesslam Abtout, Hassina Boukerbout, Boualem Bouyahiaoui, Dominique Gibert. Gravimetric evidences of active faults and underground structure of the Cheliff seismogenic basin (Algeria). *Journal of African Earth Sciences*, Elsevier, 2014, 24 th colloquium of African geology, 99 (2), pp.363-373. 10.1016/j.jafrearsci.2014.02.011 . insu-01185058

HAL Id: insu-01185058

<https://hal-insu.archives-ouvertes.fr/insu-01185058>

Submitted on 19 Aug 2015

HAL is a multi-disciplinary open access archive for the deposit and dissemination of scientific research documents, whether they are published or not. The documents may come from teaching and research institutions in France or abroad, or from public or private research centers.

L'archive ouverte pluridisciplinaire **HAL**, est destinée au dépôt et à la diffusion de documents scientifiques de niveau recherche, publiés ou non, émanant des établissements d'enseignement et de recherche français ou étrangers, des laboratoires publics ou privés.

1 Gravimetric evidences of active faults and underground structure of the Cheliff 2 seismogenic basin (Algeria)

3
4 A. ABTOUIT*, H. BOUKERBOUT*, B. BOUYAHIAOUI* , D. GIBERT**

5 *Centre de Recherche en Astronomie, Astrophysique & Géophysique –Bouzaréah, Alger, Algeria

6 ** Géosciences Rennes, CNRS/INSU (UMR 6118) & Université Rennes1, Rennes, France.
7
8
9

10 Abstract

11 The Cheliff basin (ex El Asnam) is known as one of the most seismic active zone in Algeria
12 and the West Mediterranean region. We can cite the El Asnam earthquake which occurred in
13 10.10.01980 with magnitude of 7.3. It was generated by a thrust fault with NE-SW sinistral
14 component. Until now, there is a little information about existence of deep active faults,
15 which generate this strong activity. The gravity field is an important resource of information
16 on crustal structure. The aim of this work is giving a reliable geometry of the major faults
17 relative to the kinematics of this region.

18 The results obtained from various filtered maps (derivatives, upward continuation) of the
19 gravity data, were used to generate a structural map of the studied area. Whilst the continuous
20 wavelet transform method can help in automatic detection of elongated structures in 3-D, to
21 estimate their strike direction, shape and depth. It gives a 3-D image or a model of the region
22 and confirms the existence of several faults, localised or inferred, from former geological
23 studies.

24 Keywords: Gravity anomalies, Cheliff basin, continuous wavelet transform 3-D image, deep
25 structures, faults and contacts, structural map.
26

27 1. Introduction

28 This work is carried out under the CMEP Project (Comité Mixte d'Evaluation et de
29 Prospective) which is about a geophysical and geological study of the seismogenic Cheliff
30 basin. In this study we aimed at bringing a little contribution to try to understand and placing
31 the studied area in a regional geodynamic context. This work concentrates on the relationships
32 between the various geological formations that are clearer in the basin and those bounding the
33 area and, especially the geometry of the faults at depth in relation to a general tectonic
34 context. It is based on gravity analyses correlated with complementary geological and
35 seismological information. The use of the continuous wavelet transform allows establishing a
36 3-D image of the region depicting thus a great number of deep or near surface faults and
37 contacts that had remained unknown until the present time.

38 The studied area is situated in a box ranging from $01^{\circ}00'$ – $01^{\circ}46'$ in longitude and $36^{\circ}00'$ –
39 $36^{\circ}36'$ in latitude. The region displays a complex geological setting (Figure 1) and, its
40 shallow seismicity is considered as diffuse because it spreads over a wide zone, instead of
41 indicating a single major fault (Meghraoui et al., 1996) (Figure 2). It is bounded in the North
42 by the Mediterranean Sea and in the South by the Ouarsenis Mountains which are constituted
43 by allochthonous lower Jurassic and Cretaceous formations. In the middle of the area, the E-W
44 Mio-Plio-Quaternary intra-mountainous “post-thrust” Cheliff basin overlays an ante-Neogene
45 basement consisting of Mesozoic series. It is a consequence of the distension phase that
46 occurred during the Lower-Middle Miocene (Anderson, 1936; Perrodon, 1957). The E-W
47 form of the basin implies N-S to NNW-SSE compressional movements (Meghraoui et al.,
48 1986). The structure of the Cheliff basin is the result of the Alpine orogen (Perrodon, 1957).
49 The neotectonics studies show that the main deformation is a NNW-SSE compression which
50 is related with overthrusting reverse faults and strike-slips (Groupe de Recherche
51 néotectonique de l’arc de Gibraltar, 1977; Philip and Thomas, 1977); this is confirmed by the
52 studies of African plate movements (Philip and Thomas, 1977; Minster and Jordan, 1978;
53 Anderson and Jackson, 1987) and focal mechanisms of the seismic events of 1954 and 1980
54 (Ouyed et al., 1981).

55 The main tectonic phases involving the formation of the basin is the subsidence in the Late
56 Burdigalian followed by an extensional phase in Lower Tortonian with development of
57 graben structures (Meghraoui, 1982). An important NNE-SSW compressive phase deformed
58 the Miocene formations (Meghraoui et al, 1986). In the Quaternary, a second important
59 compression phase occurred, with a NNW-SSE to NW-SE shortening direction and affected
60 the Quaternary deposits (Meghraoui, 1982). The present deformation in the Cheliff basin is
61 mainly related to a transpression with N-S to NNW-SSE shortening direction, which is
62 expressed by active tectonics responsible of the earthquake activity (Philip & Meghraoui,
63 1983, Meghraoui et al., 1986). The NE-SW trending folds and NE-SW active sinistral
64 transpressive faults were activated during the 1954 and 1980 destructive earthquakes
65 (Bezzeghoud et al., 1995; Ouyed et al., 1981). These reverse faults and related folding are
66 disposed on right lateral echelon and should be coupled with NW-SE to E-W trending strike-
67 slip deep active faults (Meghraoui, 1982, 1986, 1988; Thomas, 1985; Chiarabba et al, 1997).
68 The NE-SW faults are associated with asymmetric folds and the different tectonic structures
69 define some NE-SW blocks (Morel & Meghraoui, 1996). A kinematics model of block
70 rotation related to a transpression with NNW-SSE direction of plates convergence is proposed

71 in the Cheliff basin (Meghraoui et al., 1996) where the blocks rotation was previously studied
72 with paleomagnetic investigations by Aïfa et al., 1992 and recently by Derder et al., 2011.

73 This work complements information on some of them and outlines especially those very deep.
74 In the studied area, the Moho discontinuity is at about 30 km deep (Hatzfeld, 1978). This
75 region is integrated in a set of complex zone, in the Western Mediterranean Sea, where are
76 observed series of negative and positive gravity anomalies (Gourinard, 1958; Van Den Bosch,
77 1971; Galdeano et al., 1974; Bellot, 1985).

78 The analysis of the latest gravity survey carried out in the Cheliff region outlines a significant
79 density contrast in the South part of the basin, elongated in the NE-SW and NW-SE directions
80 (Abtout et al., 2009), which may be interpreted as a contact between the sediments up to
81 Cretaceous age of the regional stratigraphical series and the Neogene deposits of the basin.
82 Furthermore, detailed aeromagnetic data analysis of the Cheliff region, including the Cheliff
83 basin (Boukerbout et al., 2008) sketch out the presence of two major very deep E-W
84 structures localized in the North (Mediterranean Sea and along the coast) and in the South of
85 the “Cheliff” basin (Ouarsenis Mountains). Their depth is ranging between 29 and 31 km. The
86 orientation of these bounding structures does not correspond to the direction of the present
87 active faults which is mainly NE-SW.

88

89 **2. Gravity measurements and Bouguer anomaly map**

90 The gravity data were collected in different surveys carried out in this area. The data
91 distribution is not homogeneous, with a lack of information close to the coast. The
92 distribution of land measurement is irregular. It is around 0.5 km^{-2} in the Cheliff basin, except
93 in the inaccessible regions where the distribution reaches 1 km^{-2} . However, this distribution is
94 generally sufficient for our targets.

95 Therefore, all the gravity data were homogenized by linking them to the Bouzaréah station,
96 which belongs to the Algerian absolute gravity network. The data were uniformly reduced
97 with a density of 2.400 Kg m^{-3} for the Bouguer correction which is the mean density of the
98 quaternary formations, determined analytically with the use of the triplets method. The
99 topographic reduction was computed with the same uniform density and with a radius of 20
100 km.

101 The Bouguer gravity map of the studied area was produced by interpolating the entire data to
102 0.25 km grid spacing. Several interpolation methods were tested, and as there were no
103 significant differences in the resulting maps, the minimum curvature algorithm was used to
104 set up the grids that were used as a basis for later analysis.

105 Preliminary analysis of the Bouguer anomaly map determine the gravity signature of key
106 features such as the geometry of the major faults, the identification and location of the
107 geological structures and the sedimentary basin. The map (Figure 3) shows two distinct major
108 sets: in the North, positive anomalies oriented ENE-WSW, mainly due to the effect of the
109 oceanic nature of the Mediterranean crust (Auzende et al., 1973; 1975), while in the South,
110 appears the negative effect of the roots of the Ouarsenis Mountains. In the central part, a
111 series of negative anomalies located on Mio-Plio-Quaternary terrains, trending in the NE-SW
112 direction and corresponding to the Cheliff basin effect.

113

114 **3. Interpretation and discussion**

115

116 **3.1 Identification of gravity features**

117 To emphasize gravity contrasts on the Bouguer anomaly map (Figure 3), some automatic
118 structural analysis were undertaken. This kind of analysis is suitable for defining discrete
119 borders of causative bodies at depth. To underline the short wavelength anomalies which
120 reflect the signature of shallow or sub-outcropping geological structures, the technique of
121 shading the anomaly map is used (Figure 4); the advantage of this method is that it doesn't
122 modify the strength of the high frequency signature, but, as the illumination is directional,
123 certain anomalies may be unfavourably illuminated and thus not show up. This technique is
124 particularly useful for enhancing subtle linear features, which may be related to geological
125 structures. It introduces a directional bias in that features which lie perpendicular to the light
126 source are emphasized whilst those parallel to it are subdued (McDonald et al., 1992). The
127 shaded relief image of Figure 4 enhances features with a northwesterly trend which don't
128 appear on the Bouguer anomaly map. Moreover, the residual anomaly (Figure 5) is computed.
129 It is the Bouguer anomaly values minus corresponding values on the second-order polynomial
130 surface (trend) obtained by least square. The vertical gradient is computed using the Fourier
131 transform of the gravity field (Gerard and Griveau, 1972). The vertical gradient (Figure 6) is
132 used to recognize local and shallow features, while, the residual (Figure 5) underlines the
133 contacts between geological structures with contrasting densities. As well, to separate
134 between long wavelength and short wavelength anomalies the upward continuation method is
135 applied on data (Figure 7).

136 The analysis of gravimetric maps (Figures 3 - 7), show a succession of negative anomalies, in
137 the central part of the map, corresponding to the effect of the Cheliff basin and located on
138 Mio-Plio-Quaternary terrains. More details appear on the shaded map (Figure 4), which were

139 not identified on the Bouguer anomaly map, such as those anomalies trending in the NW-SE
140 direction, in the Cheliff basin and, in NNE-SSW direction in the North.

141 First kind of gravity discontinuities are related to specific geological structures (Figure 5),
142 such as the positive anomalies in the South, which are located above Cretaceous formations
143 covered partially by Tortonian post-nappes formations. At the East, two positive anomalies
144 located on the Temoulga and Rouina massifs correspond to the Jurassic substratum.

145 Second kind of discontinuities emphasizes the main gravity gradient of the area (Figure 6). In
146 general, these several discontinuities follow known and unknown faults and contacts.

147 On these two latter maps, appear in the Cheliff basin a series of three anomalies trending from
148 the NE-SW direction, in the western part of the basin, to the E-W direction in its eastern part.
149 From West to East, these three individualised blocks are limited by the Boukadir fault, El
150 Asnam fault and Oued Fodda fault.

151 The positive anomalies in the South are separated from the negative anomalies within the
152 basin by two NE-SW discontinuities corresponding probably to the Relizane and El Asnam
153 Faults, as shown on the geological map. The negative anomalies in the West of the Cheliff
154 basin are separated by a NE-SW discontinuity corresponding to the Boukadir Fault. In
155 addition to these discontinuities, appear two irregular contacts, in the opposite direction,
156 trending in the NW-SE direction and distort negative anomalies in the West. The first
157 irregular contact is thrusting the Cheliff basin in dextral way and the second one close or
158 limits the basin and the raised basement (Mattauer, 1958; Kireche, 1977; Idres et al., 1996).

159 The examination of the upward continued maps at 2, 3, 4 and 5 km, show that the most
160 negative anomalies within the basin disappear on the upward continued map at 3 km (Figure
161 7) while the positive ones in the central part and the negative one in the western part of the
162 basin persist until the continuation at the altitude of 5km. This suggests that the thickness of
163 the Cheliff basin is not flat and can be estimated between 3 and 5 km.

164

165 **3.2 Estimation of the depth**

166 The most important application in potential fields analysis is the determination of the depth
167 and the shape of the anomalies causative structures. It is also the most frequent problem
168 encountered in interpretation, especially in determining the geometry of geological bodies
169 responsible of field anomalies, at depth. So, there were and still are too many processing
170 methods developed and suggested in potential field theory, to try to solve this problem.
171 Among these investigation methods, there is modeling the observed anomalies which leads to
172 a representation of simple geometrical interfaces such as geological contacts related to depth.

173 Idres et al., (1998) attempted to model along profiles crossing the anomalies in the NW of
174 Cheliff basin. However, the modeling approach has led up to a variety of different inversion
175 algorithms (Cuer and Bayer, 1980; Tarantola, 1987; Parker, 1994; Li and Oldenburg, 1996)
176 depending on their ability to tackle with geological prior constrains to reduce the
177 nonuniqueness of solution (Pilkington, 1997; Bosch et al., 2001). On the other hand,
178 numerous analyzing methods, which do not belong to the inverse methods family defined
179 above, were developed. They transform the measured field and allow identifying and
180 characterizing the sources responsible of the observed anomalies. For instance, empirical
181 graphical techniques were proposed for determining the depth related to magnetization
182 distribution of defined shapes (Peters, 1949). Other methods based on the use of synthetic
183 model fitting were proposed, such as Werner deconvolution (Werner, 1953; Hartman et al.,
184 1971), Euler deconvolution (Thompson, 1982; Reid et al., 1990) and analytical signal
185 (Naighian, 1972; Roest et al., 1992; Nabighian et al., 2005). Developments and improvements
186 of these methods which assume a selected geometry of the source, have been realized, such as
187 the application of clustering technique for selecting appropriate solution in Euler
188 deconvolution method (Mikhailov et al., 2003), the use of vertical gradients (Marson and
189 Kligele, 1993; Debeglia and Coppel, 1997) and the study of the noise effect in data (Keating,
190 1998). Other methods derived from Euler deconvolution and analytic signal to recover the
191 shape and the depth of the sources (Huang, 1996; Stavrev, 1997; Barbosa et al., 1999; Hsu et
192 al., 1998) or the source parameter imaging method (Thurston and Smith, 1997) based on the
193 use of the local wavenumber function (Smith et al., 1998; Thurston et al., 2002; Smith and
194 Salem, 2005; Pilkington and Keating, 2006; Salem et al., 2005; 2008).

195 In this work, to localize bodies causing gravity anomalies, we use the method based on the
196 continuous wavelet transform. More than localization, the method leads to an image of
197 structures in 3-D. This method simplifies the analysis of large amounts of data (e.g., Arneodo
198 et al., 1995; Holshneider, 1995; Torresani, 1995; Mallat, 1999). Many developments were
199 performed since the first paper of Moreau et al. (1997), where the basic principles exploit the
200 homogeneity properties of potential fields to localize and identify sources of the anomalies.

201 The homogeneous degree quantifies the shape and can be compared to the structural index
202 defined in Euler deconvolution (Sailhac et al., 2000; Sailhac and Gibert, 2003). The wavelet
203 domain is the upward continuation domain of derivatives and gradients (Moreau et al., 1999;
204 Hornby et al., 1999; Vallée et al., 2004), Hilbert transforms and analytic signal (Sailhac et al.,
205 2000; Martelet et al., 2001). The wavelet theory is efficient to deal with noise (Moreau et al.,
206 1999; Sailhac and Gibert, 2003) as it was shown through different applications to gravity data

207 (Martelet et al., 2001; Fedi et al., 2004), aeromagnetic data (Sailhac et al., 2000; Boschetti et
208 al., 2004) and electromagnetic data (Boukerbout et al., 2003). A review of the theory of the
209 continuous wavelet transform in the interpretation of potential fields, with major references,
210 can be found in the article of Sailhac et al., (2009). Then, the 2-D wavelet method was
211 developed (Boukerbout and Gibert, 2006) to analyze elongated anomalies produced by
212 geological features such as faults, contacts or prismatic bodies, by the use of the ridgelet
213 functions (Candès, 1998) and the maximum entropy criteria (Tass et al., 1998; Boukerbout et
214 al., 2003) for selecting sources location. A detailed method with synthetic example and
215 application on aeromagnetic data can be found in the paper of Boukerbout and Gibert (2006),
216 where it is also shown through this application, that the ridgelet depths are in agreement with
217 Euler depths and, better than Euler method provide a sharper determination for large depths.
218 In the Cheliff basin, the structures responsible of gravimetric anomalies are shown in (Figure
219 8). It is clear that the Cheliff basin is limited in its northern and southern parts, by elongated
220 structures (1, 2, 3 and 4) with a general trending in the E-W direction. The first structure
221 limiting the Cheliff basin, in the North, is made of three segments (1, 2 and 3). In the West,
222 the segment (1) is about 36 km long; related to Tortonian and Pliocene and upper Miocene
223 formations (Figure 1) at a depth of $z = 0$ km and reaching the depth of 2 km. The second (2)
224 and the third (3) parts of the E-W structure, in the middle and the East part of the basin, are
225 associated to Tortonian and Messinian formations, and are more deep, in its northern part, the
226 depth from 4 km to 14 km and in the middle of the basin, it reaches the depth of 16 km. The
227 second structure (4) limiting the Cheliff basin, in its southern part, is associated to Neogene
228 and Tethyan substratum, is long about 59 km and at a depth varying from 0 km to 9 km. These
229 E-W structures are crossed by some N-S ones, limiting thus the Cheliff basin in its eastern and
230 western parts. In the West of the Cheliff basin, the N-S structure (5), identified near the
231 Dahra, associated to Neogene and Tethyan substratum and Pliocene and upper Miocene
232 formations, is long about 27 km and located at a depth varying from 0 km to 5 km. Eastward
233 of the Cheliff basin, the N-S structure (6), is about 18 km long. It is located nearby
234 Quaternary formations and Neogene and Tethyan substratum, between the Boumaad and the
235 Doui massifs and reaches 4 km of depth. At the left side of this structure, another NNW-SSE
236 structure (7), appears composed of two parts, long about 22 km and 18 km, reaching 8 km in
237 the South and 11 km in its northern part, corresponding to the centre of the Cheliff basin.
238 These structures cross the E-W structures (1, 2, 3 and 4) limiting the Cheliff basin, and
239 particularly, in the centre of the basin, near Oued Fodda zone, where it shifts the E-W
240 structure into two segments, and thus its depth from 14 km to 16 km. In the Western part of

241 Cheliff basin, appear two NE-SW structures. The first one (8), long about 23 km, is located
242 nearby the Boukadir anticline, in the same direction of the Boukadir fault, but more deep,
243 between 7 km and 10 km. Northward of this structure, is identified the second NE-SW one
244 (9). It is related to the anomalies laying over Neogene and Telliian substratum and Pliocene
245 and upper Miocene formations, in the limit South of the Dahra massif. Its depth varies from 1
246 km to 11 km. This structure continues until the North of the studied area, near the Tenes
247 region and reaches the 8 km of depth. It is shifted by the E-W structure (10) which depth
248 varies from 4 km to 8 km. A NW-SE (11) structure connect the two latter NE-SW (8 and 9)
249 structures in the West of the Cheliff basin, it is composed of two parallel segments. The first
250 one is located at a depth ranging between 1 km and 2 km, and the second one, between 4 km
251 and 11 km. Another NW-SE (12) structure appears in the East of the Cheliff basin,
252 overhanging the set of E-W, N-S and NNE-SSW structures. This structure is shallower and is
253 identified between 0 km and 4 km of depth. In the North of the region, appears the E-W
254 structure (10), near the coast, corresponding to the analysis of anomalies located over volcanic
255 formations and Neogene and Telliian substratum, in the Tenes region, long about 30 km and
256 reaching 8 km of depth. Eastward of this structure, appears a NE-SW structure (13), at a depth
257 reaching 5 km. All the identified structures at shallow depth outline the majority observed or
258 supposed faults and contacts as shown in the geological map (Figure 1), except for some N-S,
259 E-W, NW-SE structures and of course those very deep. These results may complete the
260 structural map of the area and, a summary of the different gravimetric features outlined in this
261 study from different analyzing methods are reported on the shaded map in figure 9. The shape
262 achieved by gravity lineaments as identified and outlined on the shaded map, agrees with the
263 theory of the structure in blocks of the Cheliff basin (Thomas, 1985; Morel and Meghraoui,
264 1996). It is shown from the correlation with the seismicity of the area (Figure 10), that
265 majority of identified structures are located on active zones. As it is shown on this map, the
266 seismicity of the region is diffuse and has no preferential direction. The superimposing of the
267 identified structures on the seismicity map shows at first a good correlation with the known
268 faults such as Boukadir fault, Oued Allalh fault, Dahra fault, Oued Fodda fault. However,
269 there are many identified structures which are correlated with seismicity by creating a
270 preferential tendency of the seismicity while there is no geological information identifying
271 these structures. We can cite for example the identified structures creating an E-W trending of
272 the seismicity, in the centre and the South of the basin. These structures are located in the
273 regions of El Abadia - Chlef in the centre of the basin and in the South it is located near the
274 limit of the Ouarsenis Mountains. Another example appears in the West of the area. This

275 structure is elongated in the NW-SE direction and is located in the area Oued Sly – Tadjenna.
276 Finally, this correlation allows us to make trend of the seismicity of the area and the lack of
277 the geological information about these structures is probably due to the fact that these
278 structures are too deep.

279

280 **4. Conclusion**

281 The Bouguer anomaly map of the Cheliff shows two main distinguished sets of anomalies.
282 The first set of positive anomalies in the North, corresponding to oceanic crust of the
283 Mediterranean Sea. The second set of negative anomalies in the South, corresponding to the
284 effect of the roots of the Ouarsenis Mountains. Over the Mio-Plio-Quaternary terrains of the
285 Cheliff basin, lays a succession of NE-SW anomalies corresponding to the basin effect.

286 Automatic structural analyses enhance more details that were not observable on the Bouguer
287 map, such as the NW-SE positive anomalies in the Cheliff basin and in the North and suggest
288 that the thickness of the Cheliff basin is not constant and flat. Different discontinuities and
289 gravity lineaments identified show good correlation with known geological structures, such as
290 the positive anomalies, where in the South correspond to Cretaceous formations and in the
291 East correspond to the Jurassic substratum. These latter were separated from the negative
292 anomalies within the basin by NE-SW discontinuities corresponding to known faults such as
293 the Relizane and El Asnam faults, while the negative anomalies in the West of the basin are
294 separated by the Boukadir fault which trends in NE-SW direction. In the NW-SE direction
295 appear two contacts, not identified in geology, the first one thrust the basin in dextral way and
296 the second one bound the basin and the raised basement in the South, which was explained by
297 different authors by an indenter which may have reoriented the Cheliff basin in its southern
298 boundaries. Elongated and deep structures are identified in the North and the South of the
299 basin, trending in the E-W direction. In North, this structure is deeper in the central part and
300 eastward of the basin than at its West. It reaches 16 km of deep, while in the South it attains 8
301 km. The summary of the identified features as outlined on the shaded map, from different
302 analyses methods and the ridgelet transform, show geometrical shape of structures delineated
303 into different polygonal forms, at large and local scales. This organization goes in the same
304 way as the theory of the structure in blocks of the Cheliff basin, as defined by many authors.
305 Also, the correlation with seismicity, shows that majority of identified gravity features are
306 located on active zones. On the other hand, many identified features are not recognized by
307 known geological structures and especially, those very deep, which remain unresolved. So,

308 this map contributes to the geological interpretation in regions where not much subsurface
309 information exists.

310

311 **Acknowledgements**

312 This work was supported by CMEP Project N°08MDU752 and benefited from discussions
313 with our colleagues. We are grateful to the reviewers for their remarks to improve this work.
314 We thank M.E.M Derder, B. Henry and S. Maouche for the useful and constructive
315 discussions.

316

317 **References**

- 318 Abtout, A., Boukerbout, H., Bouyahiaoui, B., Gibert, D. & Derder, M.E.M., 2009. Gravity
319 anomalies and structure of Cheliff seismogenic basin (Algeria). *International Earthquake*
320 *Symposium Kocaeli*, Turkey, 17-19 August 2009.
- 321 Aïfa, T., Feinberg, H., Derder, M.E.M. & Merabet, N., 1992. Rotations paléomagnétiques
322 récentes dans le bassin du Chélif (Algérie). *Comptes Rendus de l'Académie des Sciences*
323 *Paris*, 314, SII, 915-922.
- 324 Anderson, R.V., 1936. Geology in the coastal atlas of western Algeria. *Memoir Geological*
325 *Society of America*, 4, 450 p.
- 326 Anderson, H., Jackson, J., 1987. Active tectonics of the Adriatic region. *Geophys. J. R. astr.*
327 *Soc.*, 91, 937-983.
- 328 Arneodo, A., Argoul, F., Bacry, E., Elezgaray, J., and Muzy, J.F., 1995. Ondelettes,
329 multifractales et turbulences, de l'AND aux croissances cristallines. *Diderot Editeur, Paris*,
330 *184 pp. ISBN 2-84134-024-4.*
- 331 Auzende J., Bonnin, M., Olivet, J.L., 1973. The origin of the western Mediterranean Basin, *J.*
332 *Geol. Soc. Lond.* 129 607-620.
- 333 Auzende, J., Bonnin, M., Olivet, J.L., 1975. La marge Nord-Africaine considérée comme
334 marge active. *Bull. Soc. Géol. France*, 22, (4), 486-495.
- 335 Barbosa, V.C.F., Silva, J.B.C., and Medeiros, W.E., 1999. Stability analysis and improvement
336 of structural index estimation in Euler deconvolution. *Geophysics*, **64**, 48-60.
- 337 Bellot, A., 1985. Etude gravimétrique du Rif paléozoïque : la forme du massif des Beni-
338 Boussera. *Thèse Doct. ing., USTL Montpellier.*
- 339 Bezzeghoud, M., Dimitrov, D., Ruegg, J.C. & Lammali, K., 1995. Faulting mechanism of the
340 El Asnam (Algeria) 1954 and 1980 earthquakes from modeling of vertical movements.
341 *Tectonophysics* 249, 249- 266.
- 342 Bosch, M., Guillen, A., and Ledru, P., 2001. Lithologic tomography: An application to
343 geophysical data from the Cadomian belt of northern Brittany, France. *Tectonophysics*, 331,
344 197-227.
- 345 Boschetti, F., Therond, V., Hornby, P., 2004. Feature removal and isolation in potential field
346 data, *Geophys. J. Int.*, 159, 833-841, doi:10.1111/j1365-246X.2004.02293.x.

- 347 Boukerbout, H., Gibert, D., Sailhac, P., 2003. Identification of sources of potential fields with
348 the continuous wavelet transform: Application to VLF data, *Geophys. Res. Lett.*, 30(8), 1427,
349 doi: 10.1029/2003GL016884.
- 350 Boukerbout, H., and Gibert, D., 2006. Identification of sources of potential fields with the
351 continuous wavelet transform: Two-dimensional ridgelet analysis. *Journal of Geophysical*
352 *Research*, Vol. 111, B07104, doi: 10.1029/2005JB004078.
- 353 Boukerbout, H., Abtout, A., & Gibert, D. 2008. Interpretation of aeromagnetic data in the
354 Chlef region (Algeria) using the wavelet transform in the case 3-D. *Third International*
355 *scientific and practical Conference and exhibition EAGE. European Association of*
356 *Geoscientists and Engineers*. Saint Petersburg, Russia.
- 357 Candès, M., 1998. Ridgelets: Theory and Applications. *Ph.D. thesis, Dep. Of Stat., Stanford*
358 *Univ., Stanford, Calif.*
- 359 Chiarabba, C., Amato, A. & Meghraoui, M. (1997). Tomographic images of the El Asnam
360 fault zone and the evolution of a seismogenic thrust-related fold. *Journal of geophysical*
361 *Research.*, 102(B11), 24,485–24,498, doi:10.1029/97JB01778
- 362 Cuer, M., and Bayer, R., 1980. Fortran routines for linear inverse problems. *Geophysics*, 45,
363 1706-1719.
- 364 Debeglia, N., and Coppel, C., 1997. Automatic 3-D interpretation of potential field data using
365 analytic signal derivatives. *Geophysics*, 62, 87-96.
- 366 Derder, M.E.M., Henry, B., Amenna M., Bayou B., Maouche S., Besse J., Ayache M., 2011.
367 Bloc rotation tectonics recorded in the Miocene magmatic rocks of "Beni Haoua" area
368 (northern Algeria): preliminary paleomagnetic results. *European Geosciences Union, General*
369 *Assembly 2010*, Vienna, Austria.
- 370 Fedi, M., Premicieri, R., Quarta, T., Villani, A. V., 2004. Joint application of continuous and
371 discrete wavelet transform on gravity data to identify shallow and deep sources. *Geophys. J.*
372 *Int.*, 156, 7-21, doi:10.1111/j1365-246X.2004.02118.x.
- 373 Galdeano, A., Courtillot, V., Leborgne, E., Le Mouél J.L. & Rossignol J.C., 1974. An
374 aeromagnetic survey of the southwest of the western Mediterranean: description and tectonic
375 implications. *Earth Planet. Sci. Lett.*, 23, 323-336.
- 376 Gerard, A., and Griveau, P., 1972. Interprétations quantitatives en gravimétrie et magnétisme
377 à partir de cartes transformées de gradient vertical. *Geophys. Prospect.* 20, 459-481.
- 378 Gourinard, Y., 1958. Recherche sur la géologie du littoral Oranais. – *Thèse es Science,*
379 *Service de la carte géologique de l'Algérie, Alger, 200 p.*
- 380 Groupe de Recherche néotectonique de l'arc de Gibraltar, 1977. L'histoire tectonique récente
381 (Tortonien à Quaternaire) de l'Arc de Gibraltar et des bordures de la mer d'Alboran. *Bull.*
382 *Soc. Géol. France*, XIX, 3, 575-614.
- 383 Hartman, R. R., Teskey, D.J., and Friedberg, J.L., 1971. A system for rapid digital
384 aeromagnetic interpretation. *Geophysics*, 36, 891-918.
- 385 Hatzfeld, D., 1978. Etude sismotectonique de la zone de collision ibéro-maghrébine. *Thèse*
386 *d'Etat, Univ. Grenoble I, 281 p.*
- 387 Holshneider, M., 1995. Wavelets: An analysis tool. 423 pp., *Clarendon, Oxford U.K.*
- 388 Hornby, P., Boschetti, F., Horovitz, F.G., 1999. Analysis of potential field data in the wavelet
389 domain, *Geophys. J. Int.*, 137, 175-196.

- 390 Hsu, S.K., Coppens, D., and Shyu, C.T., 1998. Depth to magnetic source using the
391 generalized analytic signal. *Geophysics*, 63, 1947-1957.
- 392 Huang, D., 1996. Enhancement of automatic interpretation techniques for recognizing
393 potential field sources. *PhD thesis, Univ. of Leeds*.
- 394 Idres, M., Ydri, A. & Lefort, J.P. 1996. Proposition d'un schéma structural du bassin du Chélif
395 (Algérie) à partir de données gravimétriques. *Comptes Rendus de l'Académie des Sciences*
396 *Paris*, 322, IIa, 85-91.
- 397 Idres, M., Lefort, J.P., Aïfa, T., 1998. Modélisations gravimétriques et magnétiques des
398 structures profondes du bassin du Chélif (Algérie). *Bulletin du Service Géologique de*
399 *l'Algérie*, 9, 1, 21-32.
- 400 Keating, P.B., 1998. Weighted Euler deconvolution of gravity data. *Geophysics*, 63, 1595-
401 1603.
- 402 Kireche, O., 1977. Etude géologique structurale des massifs de la plaine du Chélif (Doui,
403 Rouina, Temoulga). *Thèse Doct. 3^e cycle*, USTHB, Alger (Algérie).
- 404 Li, Y., and Oldenburg, D.W., 1996. 3-D inversion of magnetic data. *Geophysics*, 61, 394-408.
- 405 Mallat, S., 1999. A wavelet tour of signal processing. 2nd Edition. *Academic Press*, 629 pp.
406 *ISBN 0-12-466606-X*.
- 407 Marson, I., and Kligele, E.E., 1993. Advantages of using the vertical gradient of gravity for 3-
408 D interpretation. *Geophysics*, 58, 1588-1595.
- 409 Martelet, G., Sailhac, P., Moreau, F., Diament, M., 2001. Characterization of geological
410 boundaries using 1-D wavelet transform on gravity data: Theory and application to the
411 Himalayas. *Geophysics*, 66, 1116-1129.
- 412 Mattauer, M., 1958. Etude géologique de l'Ouarsenis oriental, Algérie. *Publ. Serv. Carte*
413 *Géol. Algérie*, 758.
- 414 McDonald, A.J.W., Fletcher, C.J.N., Carruthers, R.M., Wilson, D., Evans R.B., 1992.
415 Interpretation of the regional gravity and magnetic surveys of Wales, using shaded relief and
416 Euler deconvolution techniques. *Geol. Mag.* **129** (5), pp. 523-531.
- 417 Meghraoui, M. (1982). Etude néotectonique de la région nord-est d'El-Asnam: relation avec
418 le séisme du 10 octobre 1980. *3th cycle thesis, Paris7 Univ.*, pp 210.
- 419 Meghraoui, M., Cisternas, A. & Philip, H. (1986). Seismotectonics of the lower Chelif basin:
420 structural background of the El-Asnam (Algeria) earthquake. *Tectonics*, 5, 6, 809-
421 836.
- 422 Meghraoui, M. (1988). Géologie des zones sismiques du nord de l'Algérie: Paléosismologie,
423 tectonique active et synthèse sismotectonique. *Doct. Sci. Thesis, Univ. Paris XI*,
424 356 pp.
- 425 Meghraoui, M., Morel J.L., Andrieux J. & M. Dahmani., 1996. Tectonique plio-quadernaire de
426 la chaîne tello-rifaine et de la mer d'Alboran. Une zone complexe de convergence
427 continent-continent. *Bulletin de la Société Géologique de France*, 167, 1, 141-157.
- 428 Mikhailov, V., Galdeano, A., Diament, M., Gvishiani, A., Agayan, S., Bogoutdinov, S.,
429 Graeva, E., P. Sailhac, 2003. Application of artificial intelligence for Euler solutions
430 clustering. *Geophysics*, 68, 168180, doi:10.1190/1.1543204.
- 431 Minster, J.B., Jordan, J.H., 1978. Present-day plate motions. *J. Geophys. Res.*, 83, 5331-5354.
- 432 Moreau, F., Gibert, D., Holschneider, M., Saracco, G., 1997. Wavelet analysis of potential
433 fields, *Inverse Probl.*, 13, 165-178.

- 434 Moreau, F., Gibert, D., Holschneider, M., Saracco, G., 1999. Identification of sources of
435 potential fields with the continuous wavelet transform: Basic theory, *J. Geophys. Res.*, 104,
436 5003-5013.
- 437 Morel, J.L. & Meghraoui, M., 1996. Goringe-Alboran-Tell tectonic zone; a transpression
438 system along the Africa-Eurasia plate boundary. *Geology*, 1996, 24, 8, 755-758.
- 439 Nabighian, M.N., 1972. The analytic signal of two-dimensional magnetic bodies with
440 polygonal cross-section. *Geophysics*, 37, 507-517.
- 441 Nabighian M.N., Grauch, V.J.S., Hansen, R.O., 2005. The historical development of the
442 magnetic method in exploration. *Geophysics*, 70, 33-61.
- 443 Ouyed, M., Meghraoui, M., Cisternas, A., Deschamp, A., Dorel, J., Frechet, F., Gaulon, R.,
444 Hatzfeld, D. & Philip, H. 1981. Seismotectonics of the El Asnam earthquake. *Nature*, 292,
445 5818, 26-31.
- 446 Parker, R.L., 1994. Geophysical Inverse Theory. *Princeton Univ. Press, Princeton, N.J.*
- 447 Perrodon, A., 1957. Etude géologique des bassins néogènes sublittoraux de l'Algérie du
448 Nord occidental. *Publications du service de la carte géologique de l'Algérie*, 12, 343.
- 449 Peters, L. J., 1949. The direct approach to magnetic interpretation and its practical application.
450 *Geophysics*, 14, 290-320.
- 451 Philip, H. & Meghraoui, M., 1983. Structural analysis and interpretation of the surface
452 deformations of the El-Asnam earthquake of October 10, 1980. *Tectonics*, 2, 1, 17-49.
- 453 Philip, H., Thomas, G., 1977. Détermination de la direction de raccourcissement de la phase
454 de compression quaternaire en Oranie (Algérie). *Rev. Géogr. Phys. Géol. dyn.*, 19, (4), 315-
455 324.
- 456 Pilkington, M., 1997. 3-D magnetic imaging using conjugate gradients. *Geophysics*, 62, 1132-
457 1142.
- 458 Pilkington, M., and Keating, P., 2006. The relationship between local wavenumber and
459 analytic signal in magnetic interpretation. *Geophysics*, 71, 1.1-1.3, doi:10.1190/1.2163911.
- 460 Reid, A.B., Allsop, J.M., Granser H., Millet, A.J., and Somerton, I.W., 1990. Magnetic
461 interpretation in three dimensions using Euler deconvolution. *Geophysics*, 55, 80-91.
- 462 Roest, W.R., Verhoef, J., and Pilkington, M., 1992. Magnetic interpretation using the 3-D
463 analytic signal. *Geophysics*, 57, 116-125.
- 464 Sailhac, P., Galdeano, A., Gibert, D., Moreau, F., Delor, C., 2000. Identification of sources of
465 potential fields with the continuous wavelet transform: Complex wavelets and application to
466 aeromagnetic profiles in French Guiana. *J. Geophys. Research*, 105, 19455–19475.
- 467 Sailhac, P., Gibert, D., 2003. Identification of sources of potential fields with the continuous
468 wavelet transform: Two-Dimensional wavelets and multipolar approximation, *J. Geophys.*
469 *Res.*, 108(B5), 2262, doi: 10.1029/2002JB002021.
- 470 Sailhac, P., Gibert, D., Boukerbout, H., 2009. The theory of the continuous wavelet transform
471 in the interpretation of potential fields: a review. *Geophysical Prospecting*, Vol. 57, No. 4. pp.
472 517-525.
- 473 Salem A., Ravat, D., Smith, R.S., and Ushijima, K., 2005. Interpretation of magnetic data
474 using an enhanced local wavenumber (ELW) method. *Geophysics*, 70, no. 2, 7-12.
- 475 Salem, A., Williams, S., Fairhead, D., Smith, R.S., and., Ravat, D., 2008. Interpretation of
476 magnetic data using tilt-angle derivatives. *Geophysics*, 73, 1-10.

- 477 Smith, R.S., Thurston, J.B., Dai, T., and Macleod, I.N., 1998. iSPI - The improved source
 478 parameter imaging method. *Geophysical Prospecting*, 46, 141-151.
- 479 Smith, R.S., and Salem, A., 2005. Imaging depth, structural and susceptibility from magnetic
 480 data: The advanced source-parameter imaging method. *Geophysics*, 70, no. 4, 141-151.
- 481 Stavrev, P.Y., 1997. Euler deconvolution using differential similarity transformations of
 482 gravity or magnetic anomalies. *Geophys. Prosp.*, 45, 207-246.
- 483 Tass, P., Roseblum, M. G., Weule, J., Kurths, J., Pikovsky, A., Volkmann, J., Schnitzler, A.,
 484 Freund, H.-J., 1998. Detection of n:m phase locking from noisy data: application to magneto
 485 encephalography. *Phys. Rev. Lett.*, 81, 3291-3294.
- 486 Tarantola, A., 1987. Inverse Problem Theory. *Elsevier, New York*.
- 487 Thomas, G. 1985. Géodynamique d'un bassin intra montagneux: le bassin du bas Chéiff
 488 occidental (Algérie) durant le Mio-Plio-Quaternaire. *Doct. Sci. Thesis, Univ. de Pau, France*.
- 489 Thompson, D. T., 1982. EULDPH: A new technique for making computer-assisted depth
 490 estimates from magnetic data. *Geophysics*, 47, 31-37.
- 491 Thurston, J.B., and Smith, R.S., 1997. Automatic conversion of magnetic data to depth, dip
 492 and susceptibility contrast using the SPI method. *Geophysics*, 62, 807-813.
- 493 Thurston, J.B., Smith, R.S., and Guillon, J., 2002. A multi-model method for depth
 494 estimation from magnetic data. *Geophysics*, 67, 555-561.
- 495 Torresani, B., 1995. Analyse continue par ondelettes. *InterEditions & CNRS Editions, Paris*.
 496 239 pp. ISBN 2-7296-0591-6.
- 497 Vallée, M.A., Keating, P., Smith, R.S., and St-Hilaire, C., 2004. Estimating depth and model
 498 type using the continuous wavelet transform of magnetic data. *Geophysics*, 69, 191-199.
- 499 Van Den Bosch, J.W.H., 1971. Carte gravimétrique du Maroc au 1/500000, Anomalie de
 500 Bouguer $d = 2.67$. – *Notes et Mém. Serv. Géol. Maroc, n° 234*.
- 501 Werner, S., 1953. Interpretation of magnetic anomalies at sheet-like bodies. *Serviges*
 502 *Geologiska Undersok, Ser. C, 43, N06*.

503

504 **List of figures**

505

506 Figure 1. Localization and geological setting of the Cheliff region (modified from Meghraoui,
 507 1988). The studied area (four-sided white figure) is located in a box ranging from 01° -
 508 $01^{\circ}46'$ in longitude and 36° - $36^{\circ}36'$ in latitude.

509 Figure 2. Seismotectonic map of the NW of Algeria.

510 Figure 3. The Bouguer anomaly map of the studied area based on 0.25 km grid spacing of
 511 data reduced with density of 2.400 kg m^{-3} .

512 Figure 4. Shaded map of the Bouguer anomaly. This map enhances more details that not
 513 appear on the Bouguer map and, allow a best correspondence with geological features.

514 .Figure 5. The residual map of the Bouguer anomaly, showing shallow known and unknown
 515 contacts between geological structures with contrasting densities.

516 Figure 6. Vertical gradient of the Bouguer anomaly. High frequency anomalies are visible in
517 the Cheliff basin corresponding to faults and contacts.

518 Figure 7. Upward continuation at 3 km of the Bouguer anomaly showing large wavelengths.
519 The most negative anomalies within the basin disappear on the upward continued map at 3 km

520 Figure 8. 3-D image of identified structures located by ridgelet analysis of the gravity
521 anomalies. The North direction is given by the latitude axis. The colour scale corresponds to
522 the maximum entropy criteria (Tass et al., 1998; Boukerbout et al., 2003; Boukerbout and
523 Gibert, 2006; Sailhac et al., 2009) for selecting sources location.

524 Figure 9. Summary of the different gravimetric features outlined from different analyzing
525 methods reported on the shaded map: in white those identified from residual and vertical
526 gradient; in colour those identified from ridgelet analysis which are represented by an image
527 plane of the perspective on Figure 8.

528 Figure 10. Correlation between gravimetric identified structures from different analysis
529 methods and the seismicity map of the studied area. The identified structures such as
530 summarized on Figure 9, are superimposed on the seismicity map to do the correlation.

531

532

533

534

535

536

537

538

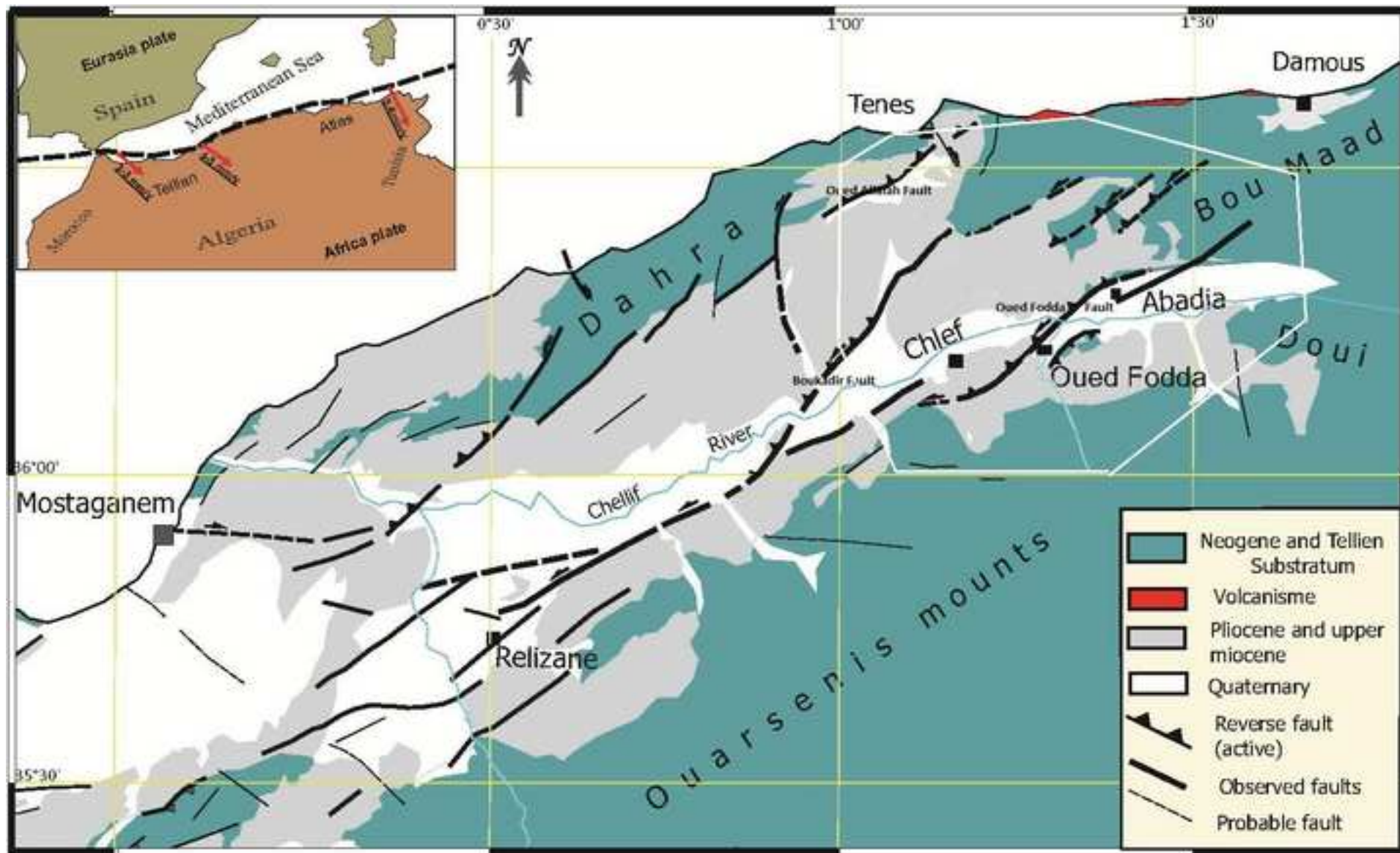
539

540

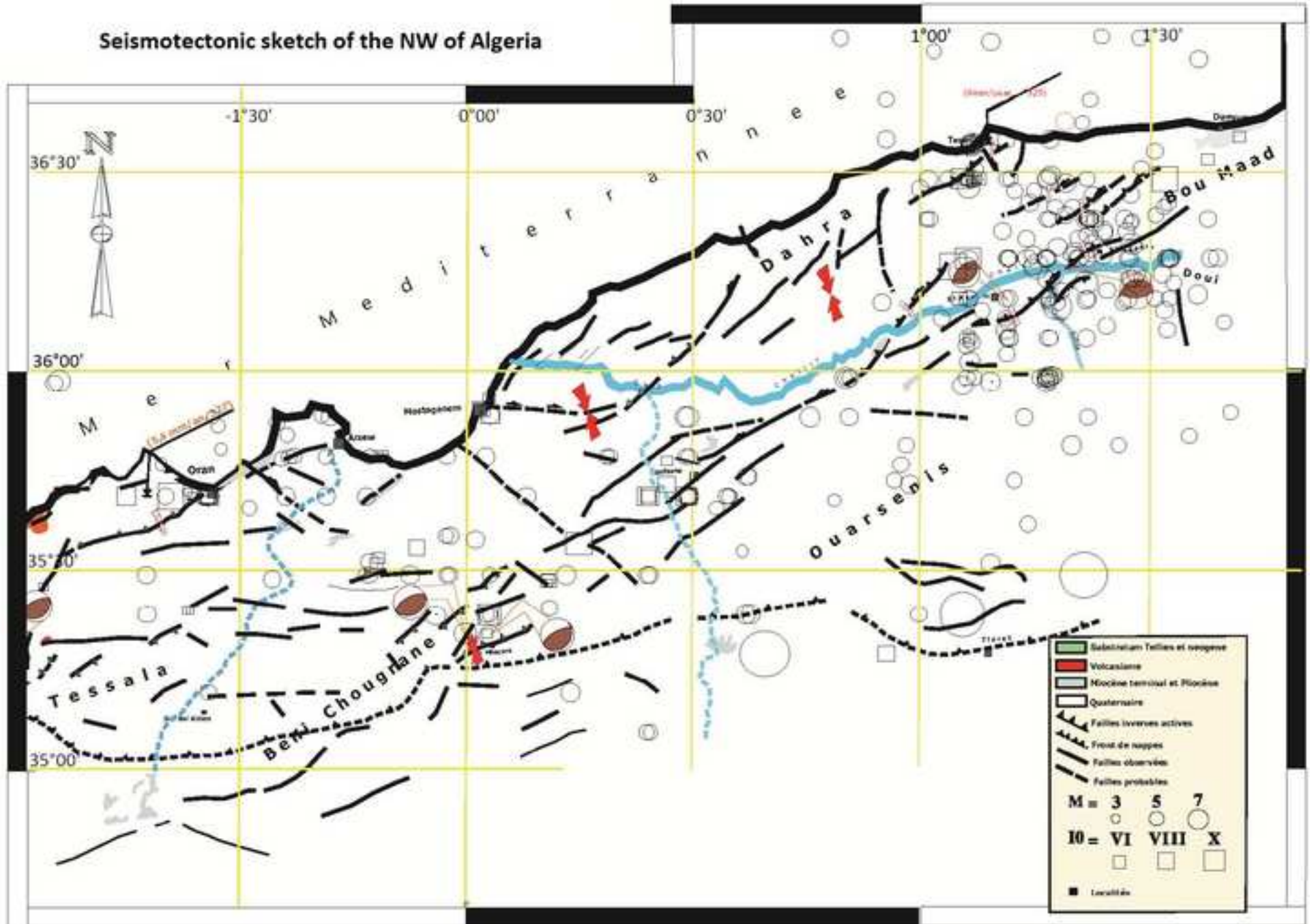
541

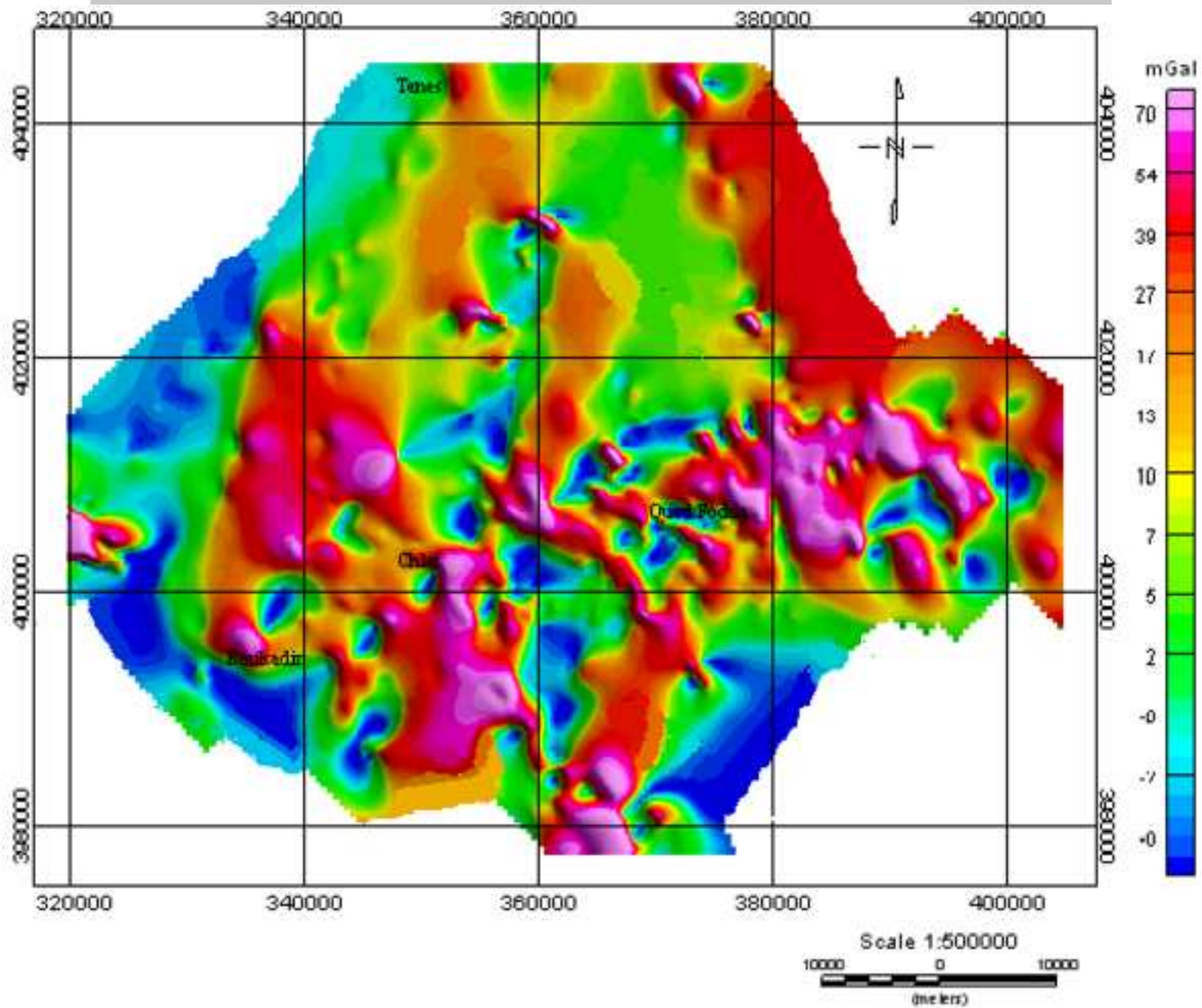
542

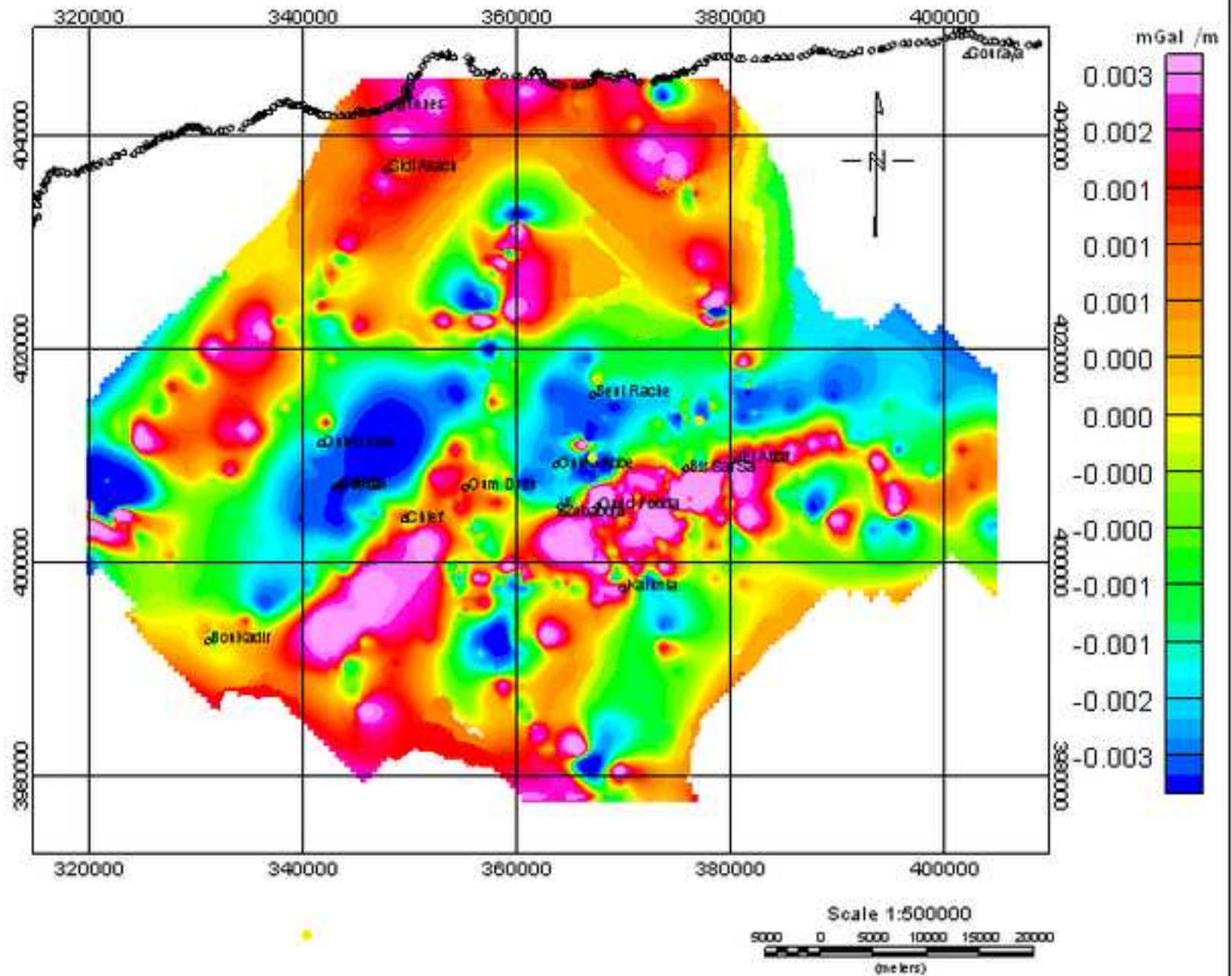
543

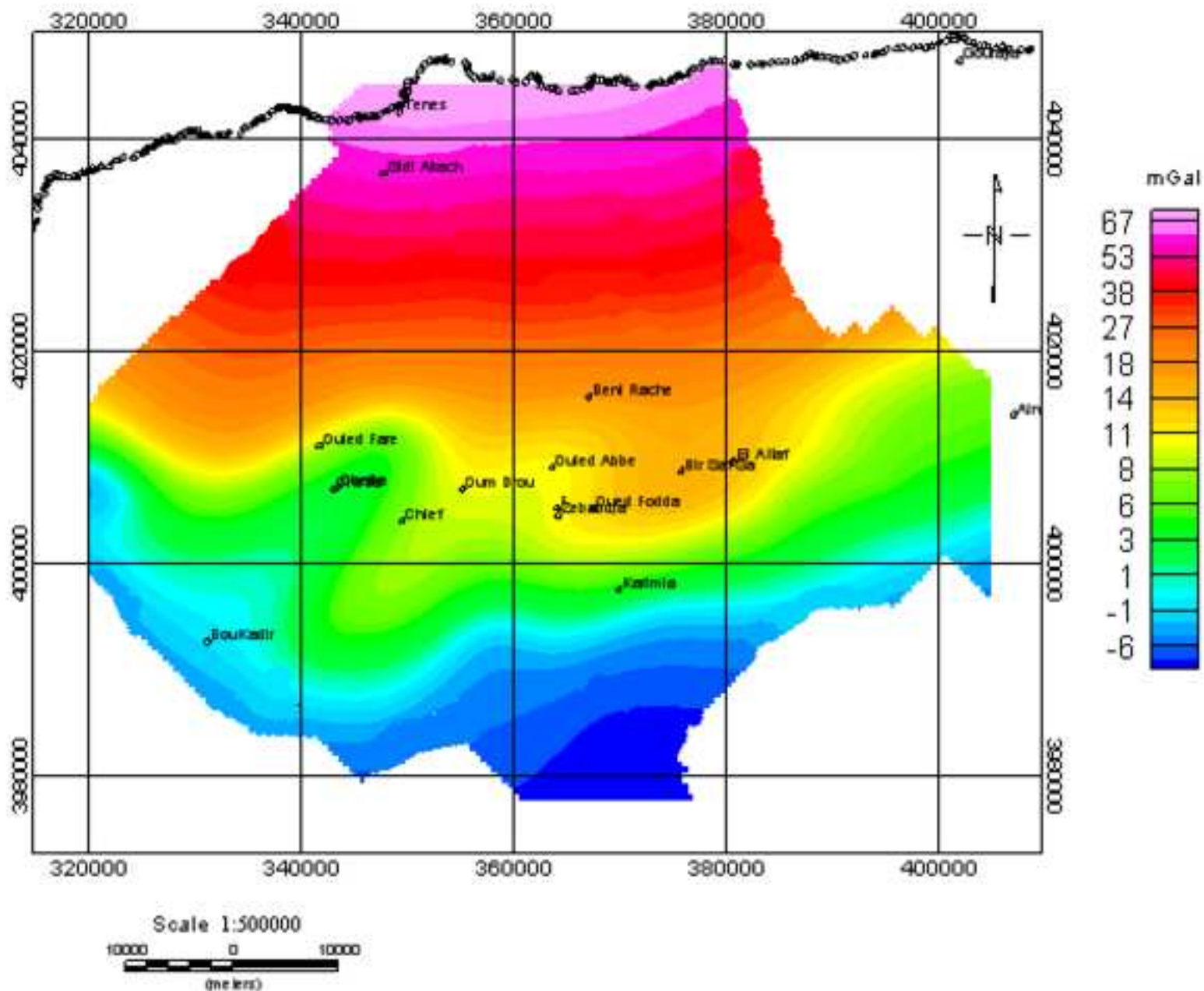


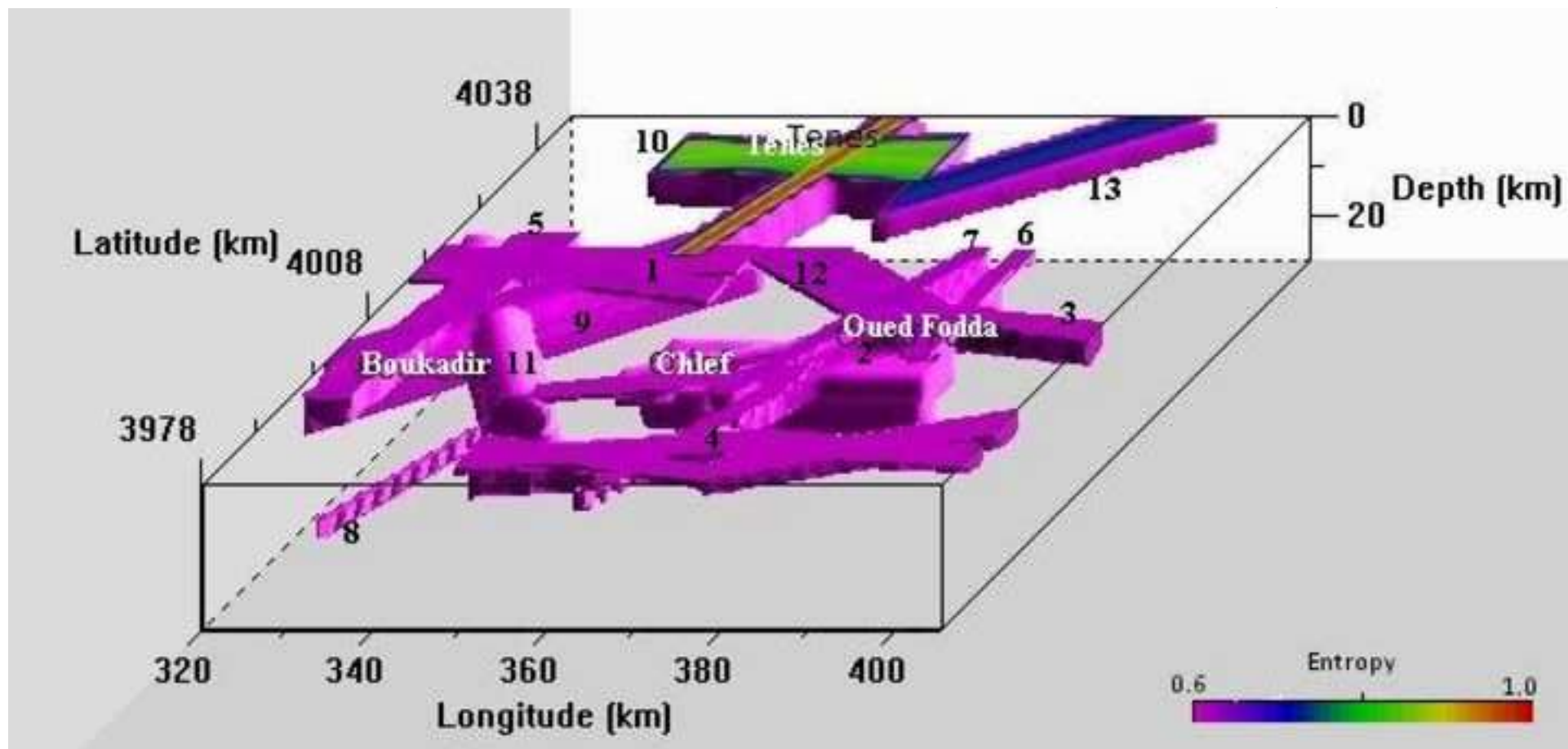
Seismotectonic sketch of the NW of Algeria

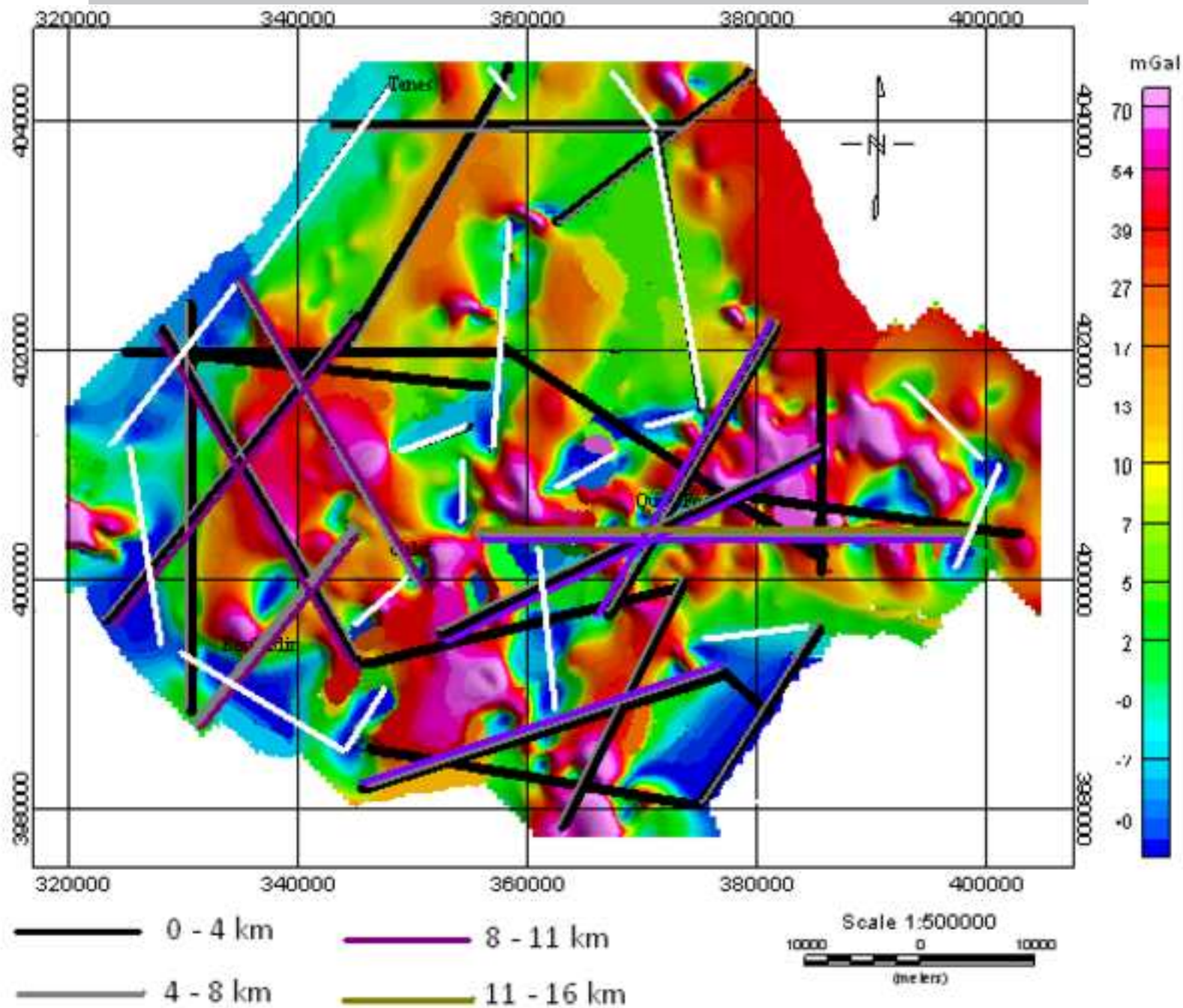


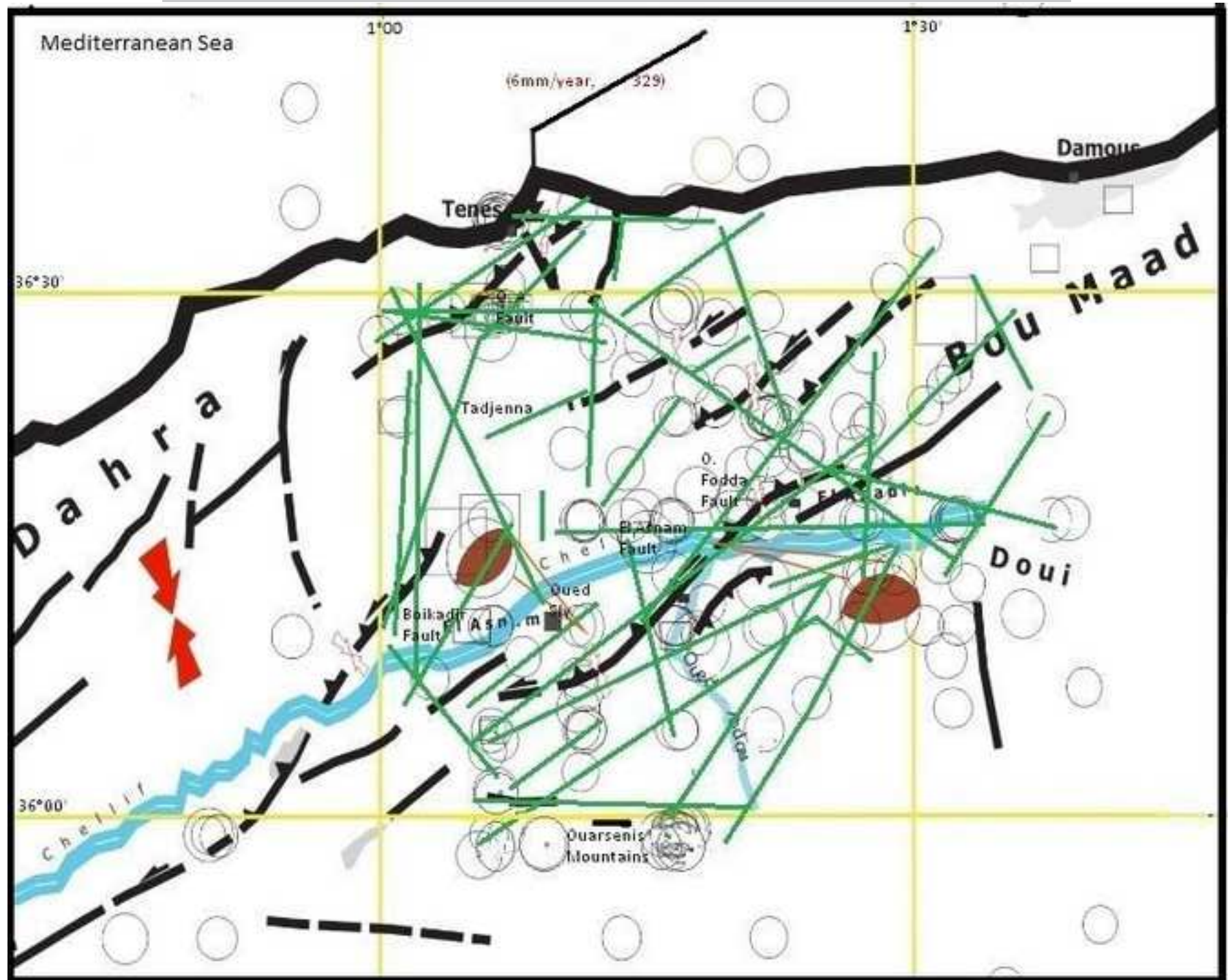












Highlights

1
2 We study gravity anomalies of the seismogenic Cheliff region in Algeria.
3 We use different processing methods to highlight long and short wavelength.
4 We use the continuous wavelet transform to identify deep anomalies causative bodies.
5 We establish the 3-D image of Cheliff basin
6 A correlation between geological, seismotectonic data and gravity features is done.
7
8
9
10
11
12
13
14
15
16
17
18
19
20
21
22
23
24
25
26
27
28
29
30
31
32
33
34
35
36
37
38
39
40
41
42
43
44
45
46
47
48
49
50
51
52
53
54
55
56
57
58
59
60
61
62
63
64
65

ACCEPTED MANUSCRIPT